Available online at www.sciencedirect.com
ScienceDirect
Polymer 48 (2007) 2778–2790
polymer
www.elsevier.com/locate/polymer

Morphology evolution during injection molding: Effect of packing pressure

R. Pantani*, I. Coccorullo, V. Speranza, G. Titomanlio

Department of Chemical and Food Engineering, University of Salerno, via Ponte don Melillo, I-84084 Fisciano (Salerno), Italy

Received 24 November 2006; received in revised form 1 March 2007; accepted 2 March 2007
Available online 7 March 2007

Abstract

Injection molding is one of the most widely employed methods for manufacturing polymeric products. The final properties and then the quality of an injection molded part are to a great extent affected by morphology. Thus, the prediction of microstructure formation is of technological importance, also for optimizing processing variables. In this work, some injection molding tests were performed with the aim of studying the effects of packing pressure on morphology distribution. The resulting morphology of the moldings was characterized and it was compared with previous results gathered on samples obtained by applying a lower holding pressure. Furthermore, the molding tests were simulated by means of a code developed at University of Salerno. The results obtained show that on increasing holding pressure the molecular orientation inside the samples increases, and simulations show that this is due mainly to the increase of relaxation time caused by the higher pressures. On discussing the simulation results, some considerations are made on the effects of pressure on crystallization kinetics and on rheology.

Keywords: Injection molding; Packing pressure; Morphology

1. Introduction

The thermomechanical conditions imposed during polymer processing affect the morphological characteristics of the final object, which are essentially dictated by crystallinity degree, molecular orientation and crystal structure and dimensions, thus determining its final properties [1]. In the case of injection molding, one of the most widely employed methods for manufacturing polymeric products, the combined effect of processing variables, part geometry, type of flow and thermo-rheological properties of the material create specific fields of pressure, temperature, shear rate and stress. On their turn, these ones cause a peculiar distribution of morphology and thus of physical and chemical properties inside the injection molded part thus determining the product quality [2]. Needless to mention, the prediction of microstructure formation in semi-crystalline polymers is of extreme technological importance. Furthermore, an accurate simulation of injection molding can cut down the expensive costs of tooling and of trial-and-error mold testing. Exhaustive reviews on the state of the art on morphology development in injection molding can be found in Refs. [3–5].

Recently, a thorough analysis of the effect of operative conditions on morphology distribution in injection molded polypropylene samples was presented [3]: the effect of flow rate and mold temperature was analyzed. That analysis is further carried out in this work, in particular, analyzing the effects of packing pressure on morphology distribution. For this goal to be achieved, some injection molding tests were performed adopting the same isotactic polypropylene of the previous work [3], but adopting a higher holding pressure.

In general, under high pressures, rheological characteristics and the temperatures of crystallization (and consequently the crystallization kinetics) of iPP change dramatically [6,7].

* Corresponding author. Tel.: +39 089 964141; fax: +39 089 964057.
E-mail address: rpantani@unisa.it (R. Pantani).

0032-3861/$ - see front matter © 2007 Elsevier Ltd. All rights reserved.
doi:10.1016/j.polymer.2007.03.007

The morphology of the moldings was characterized in this work by adopting different experimental techniques and, with the aim of underlining the effects of holding pressure, it is compared with previous results gathered from samples obtained with lower holding pressures.

2. Experimental results

2.1. Material

A commercial grade iPP resin (T30G, Mw = 376,000, Mw/Mn = 6.7, tacticity = 87.6%mmmm), kindly supplied by Montell (Ferrara, Italy) was adopted for the experiments. This material is the same as the one adopted by Titomanlio and co-workers [3,8] to analyze effects of flow rate and mold temperature on morphology distribution of injected samples and the effects of pressure on crystallization [9].

2.2. Injection molding

Experiments were performed on a 65-ton Penta injection molding machine equipped with an instrumented mold. The material was injected into a line gated rectangular cavity of $120 \times 30 \times 2$ mm^3. The molding machine and the mold were equipped with five piezoelectric transducers: one in the injection chamber, one just before the gate and three in the cavity, located in the non-moving part of the mold (15, 60 and 105 mm downstream from the gate). These positions will be referred to as P0, P1, P2, P3 and P4, respectively. A complete description of mold geometry is reported elsewhere [3,10]. As already mentioned, in a previous work [3] some injection molding tests were performed on the isotactic polypropylene T30G. One of the tests was performed with nominal injection flow rate of 15 cm^3/s, holding pressure of 400 bar, holding time of 10 s, mold temperature of 298 K, melt temperature of 503 K. This sample was considered as a reference in order to evaluate the effects of an operating condition change on the crystallinity and microstructure distribution in the molding; thus, its molding conditions, reported in Table 1, are denoted as ''standard'' in the following. In order to study holding pressure effects, an additional molding test was performed, in which a higher holding pressure was applied (700 bar), all other variables were left unchanged with respect to the ''standard'' sample, as reported in Table 1.

Experimental pressure curves in the five transducer positions are reported in Fig. 1a for the ''standard'' and Fig. 1b for the ''high P'' samples. As expected, a higher holding pressure induces much higher pressure levels inside the cavity and, due to the effect of pressure on viscosity, higher pressure drops between transducer positions. Furthermore, inside the cavity, just downstream from the gate, a residual pressure was still present at mold opening when a holding pressure of 700 bar was adopted.

Table 1
Molding conditions

Processing parameters	''Standard''	''High P''
Flow rate [cm^3/s]	15	15
Mold T [K]	298	298
Holding P [bar]	400	*700*
Injection T [K]	503	503

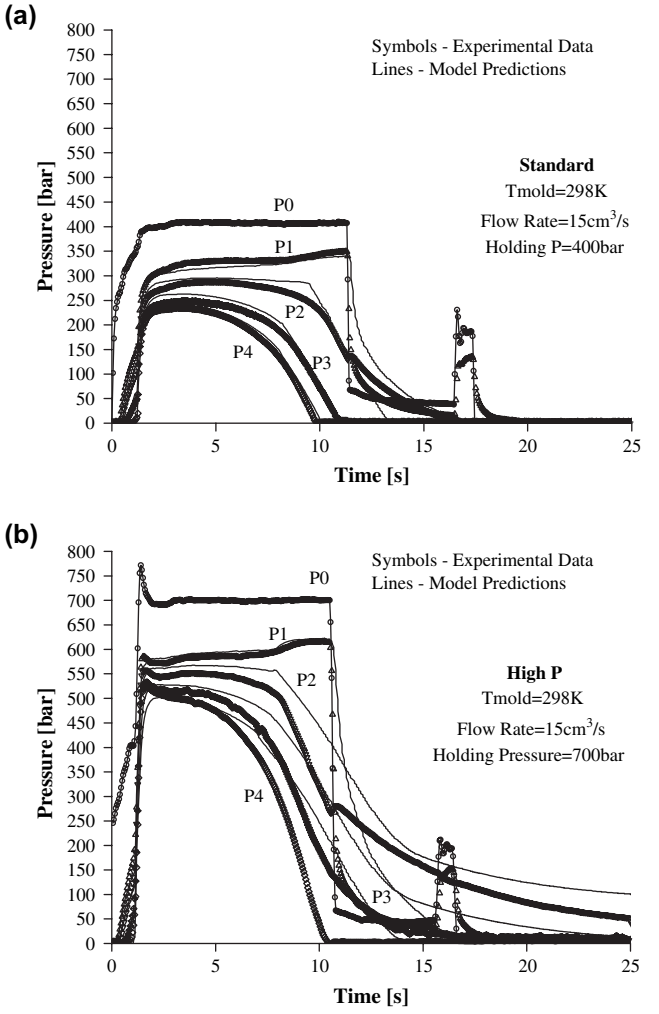

Fig. 1. Simulated and experimental pressure curves for both ''standard'' and ''high P'' samples.

It has been reported [11] that an inflection point in the pressure evolution just upstream from the gate (Pos. P1 in Fig. 1a and b) takes place when the gate solidifies. Correspondingly, the pressure curve just downstream from the gate (Pos. P2) changes its concavity from downward to upward. Thus, pressure evolution curves reported in Fig. 1a and b are consistent with gate solidification times of about 10 s for the standard and 8 s for the high P sample. A higher holding pressure seems thus to induce an earlier gate solidification.

2.3. Analysis of morphology distribution

For crystallinity and morphology investigations, thin slices were cut by means of a Leica slit microtome from molded samples at the positions where pressure transducers were located inside the cavity, P2–P3–P4. The slices were cut along

the flow direction and parallel either to the flow-thickness plane (referred to in the following as scheme A) or to the flow-width plane (scheme B). Slices cut according to scheme A refer therefore to a full thickness (=2 mm) section of the sample and were cut at 15 mm from sample lateral surface. Vice versa, slices cut according to scheme B refer to sections at different distances from sample skin.

In order to study morphology distribution along flow and thickness directions, thin slices cut from injected samples according to scheme A in P2, P3 and P4, were analyzed by polarized light optical microscopy, SEM, AFM and infrared analysis.

2.3.1. Morphology distribution along thickness direction

Micrographs in polarized optical light of slices cut in P3 (central position in cavity) according to scheme A from both ''standard'' and ''high P'' samples are reported in Fig. 2. Two series of micrographs are reported in the figure: in Fig. 2a, the slices are oriented so that flow direction is aligned along the analyzer direction; in Fig. 2b, the same slices are rotated 45°. Normally, the change of brightness during a 45° rotation is directly proportional to the material orientation level. The micrographs show a morphology distribution typical of an injection molded semi-crystalline sample, often referred to as skin-core morphology. They reveal the presence of a series of distinct regions: a thin row nucleated layer; a highly oriented non-spherulitic zone (shear layer); a spherulitic core. The effect of packing pressure on the shear layer thickness of the moldings can be determined from Fig. 2: the thickness of the shear layer in the ''high P'' sample is slightly larger than the one in the ''standard'' sample. The effect has to be caused by the packing flow, because the filling step was the same for both tests. Indeed, the effect of flow on orientation is enhanced by a pressure increase, as both relaxation times and packing flow increase with pressure. It is therefore expected that the layers solidified during the packing step are more oriented in the ''high P'' sample than in the ''standard'' sample.

In order to better characterize the skin-core morphology, the same slices were chemically etched [12] and then observed using both scanning electronic and atomic force microscopy. AFM micrographs are reported in Fig. 3 (for ''standard'' sample) and in Fig. 4 (for ''high P'' sample): the first micrograph of each figure refers to shear zone of Fig. 2 and the second one to the central layer (sample midplane). AFM observations confirm results obtained by optical microscopy for all samples analyzed: internal layers resulted to be fully spherulitic whereas inside the dark zone of Fig. 2 highly oriented structures (fibers) were observed and spherulites could not be detected.

Micrographs were used to evaluate distribution of spherulite diameter along thickness direction in position P3, central in cavity: results are reported in Fig. 5 for the ''high P'' sample. In order to highlight the effect of packing pressure on spherulite dimensions, results of the standard sample are also reported in Fig. 5.

The figure shows that, consistently with literature indications, the largest spherulites are in the core region and spherulite diameters become smaller from the core region toward the skin. Holding pressure does not seem to influence spherulite dimensions at the midplane, whilst, at intermediate layers (about 0.7 mm from the skin), on increasing packing pressure the spherulite dimensions undergo a slight decrease.

2.3.2. Morphology distribution along flow direction

Morphology distribution along flow direction was studied by observing slices cut according to scheme A in the three positions (P2, P3 and P4) where pressure transducers were located. Micrographs obtained in polarized light of slices cut according to scheme A are reported in Fig. 6 for the ''standard'' sample and in Fig. 7 for the ''high P'' sample.

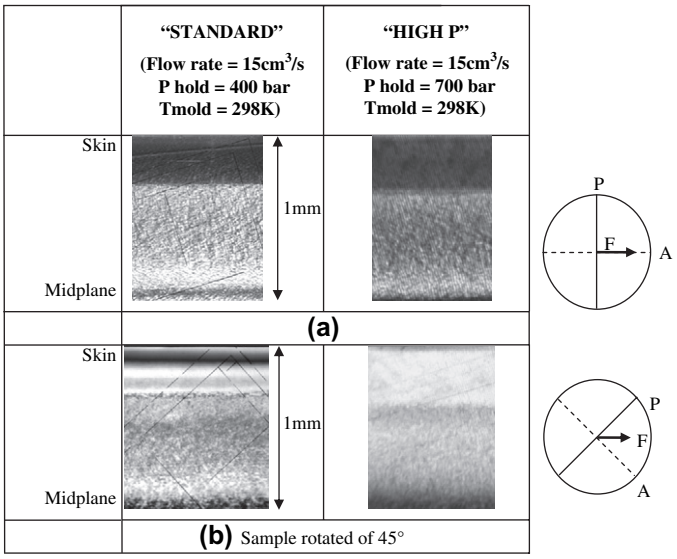

Fig. 2. Optical micrographs in P3. The alignment of the samples between crossed polarizers is reported on the right: ''A'' represents the analyzer; ''P'', the polarizer; ''F'', the flow direction.

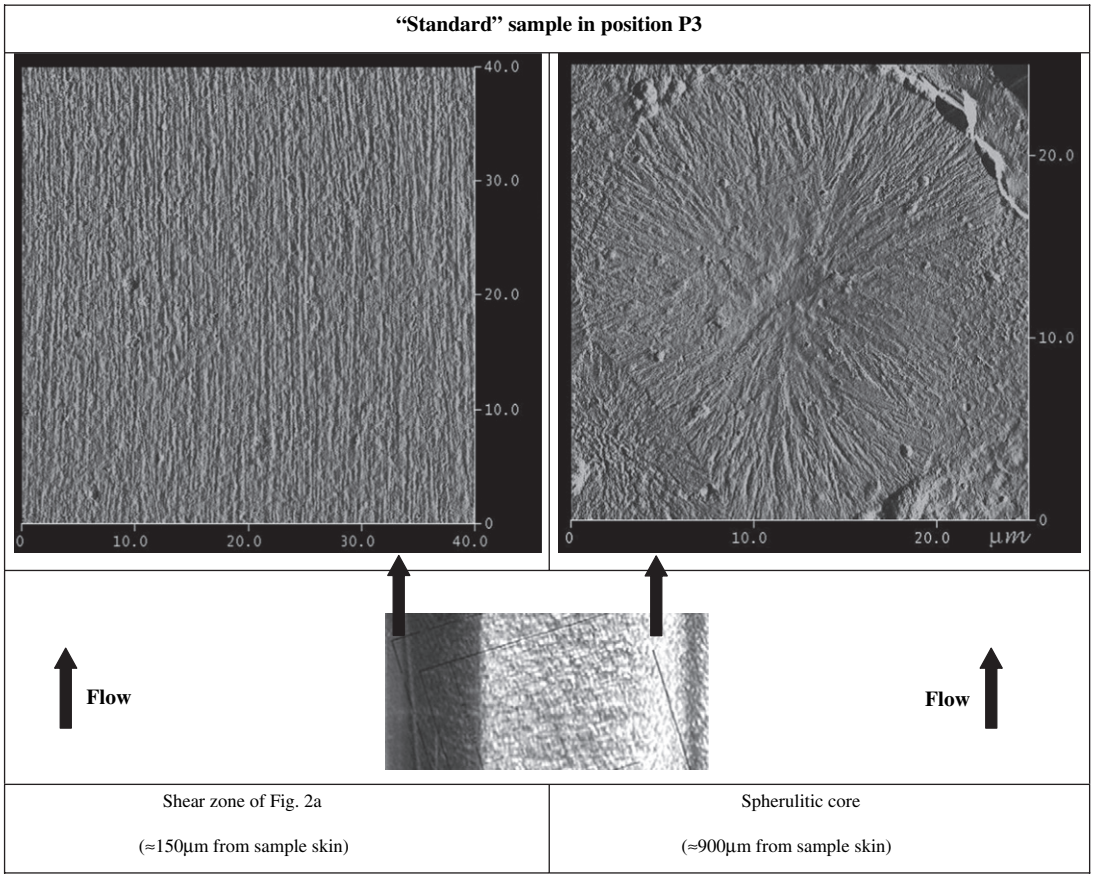

Fig. 3. AFM images of "standard" sample.

The micrographs confirm that the skin-core morphology observed in P3 is present also in the other positions along the flow direction. Values of the thickness of the oriented region (skin layer and shear zone), δ, are shown in Fig. 8 as a function of the position along the flow direction. Consistently with literature [4], the skin layer thickness increases with the distance from the gate, goes through a maximum at the intermediate x-location, and then decreases toward the tip of the cavity. Results reported in Fig. 8 show that, on increasing packing pressure, the thickness of the shear layer slightly increases at all positions considered.

2.4. Crystallinity distribution

2.4.1. FTIR analysis

Slices microtomed from injected samples parallelly to the sample skin (scheme B) were analyzed by means of an IR spectrophotometer (Brucker device). The crystallinity degree distribution was determined by the analysis of the FTIR absorbance spectra applying Lambert and Beer's law to selected peaks [13]. The procedure is reported elsewhere [3]. FTIR analysis does not allow to discriminate between different crystalline phases and thus the crystallinity degree as measured by FTIR analysis has to be considered as an overall value accounting for all existing crystalline phases.

Results of overall crystallinity distribution along thickness in P3 obtained on the "high P" sample by means of IR analysis are reported in Fig. 9 and, consistently with results obtained by analyzing "standard" sample (Fig. 10), they show that the final overall crystallinity degree is about constant along thickness, in spite of the very high cooling rates experienced by the polymer close to sample skin. This behavior is consistent with literature indications: Piccarolo et al. [14], analyzing the effect of pressure on crystallinity, observed that, on increasing pressure, the decrease of alpha phase is mainly balanced by an increase of the mesomorphic phase content, whilst the amorphous phase is only slightly affected by the pressure increase; namely the overall crystallinity degree is not influenced by the pressure.

2.4.2. X-ray analysis

Some of the thin slices cut according to scheme B in position P3 were analyzed by WAXD. Some WAXD patterns are reported in Fig. 11. In Fig. 11a and e a very weak nearly-isotropic ring is observed for the 110 peak, resulting from a fraction of crystallites that are not highly oriented, in spite of the very high stress experienced by the polymer close to the sample skin.

Diffraction patterns reported in Fig. 11b and f, correspond to positions in the shear zone: they are characteristic of the

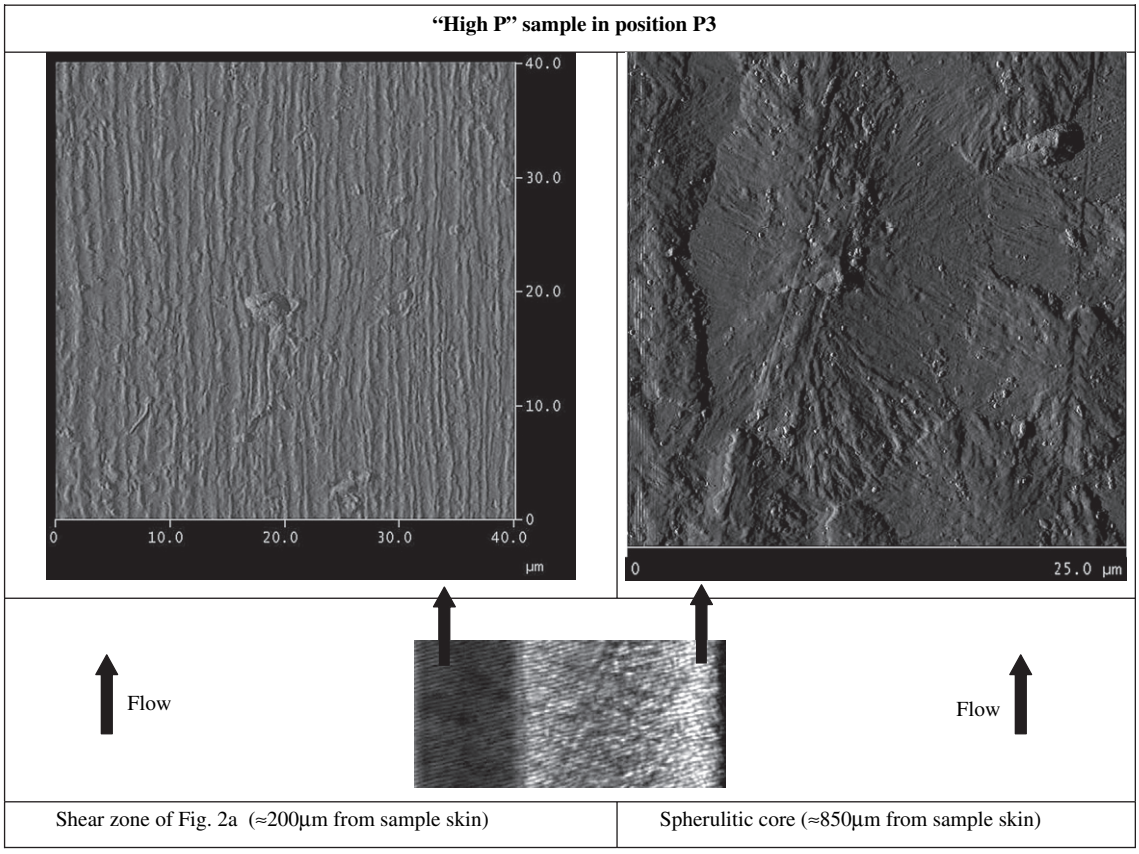

Fig. 4. AFM images of "high P" sample.

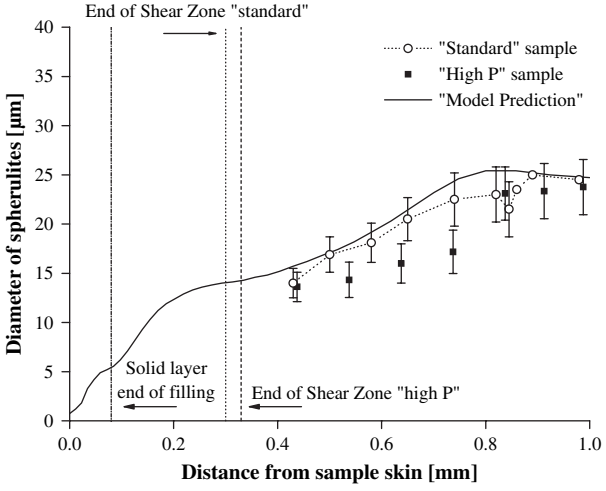

Fig. 5. Spherulite diameters obtained by SEM analysis vs distance from sample skin in position P3 for both "standard" and "high P" samples. Lines refer to model predictions.

monoclinic crystalline unit cell of the α-phase and have a bimodal character. This distinctive pattern is unique to isotactic polypropylene and is attributed to the crystallographic branching of "daughter" lamellae growing epitaxially with their *a*- and *c*-axes parallel to the *c*- and *a*-axes of the "parent" lamellae, respectively (see Fig. 12).

Two-dimensional WAXD patterns (such as those in Fig. 11) can be circularly averaged to generate plots of diffracted intensity as a function of angle 2θ. Diffractograms relative to the "standard" sample show the main peaks at 14.1°, 16.8°, 18.6° and 22° of 2θ, characteristic of the monoclinic α form of all slices analyzed. Diffractograms relative to the "high P" sample show, in addition to the main peaks characteristic of the α form, also small peaks characteristic of the γ form (16.71°, 21.86°). As already reported [14], this behavior could be explained with the enhancement of the formation of the γ form on increasing pressure. WAXD patterns were also analyzed by a deconvolution procedure [15]. Results of the deconvolution procedure performed on WAXD patterns are reported in Figs. 9 and 10. A comparison between the two figures shows that the ratio between the mesomorphic phase and the α-phase increases in the whole thickness when high holding pressure is applied. Moreover, for high P samples, the percentage of the γ-phase is close to 5% essentially on the whole sample thickness. It is worth mentioning that no increase of mesomorphic content is detected at the sample skin, in spite of the very high cooling rates experienced by the polymer in that region.

In order to analyze crystallinity degree distribution along flow direction, IR analysis was performed also on slices cut according to scheme B in positions coded as P2 and P4 (1.5 and 10.5 cm from the gate). Results (not reported here) confirm that the final overall crystallinity degree is about

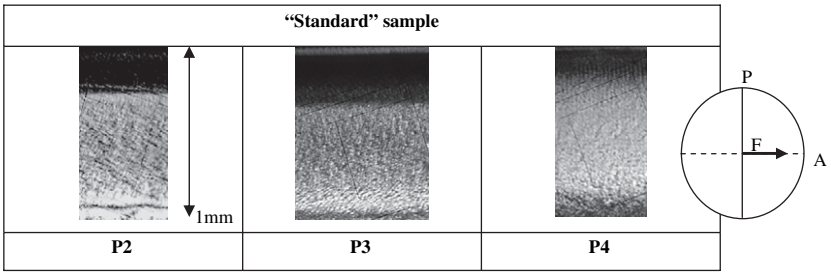

Fig. 6. Micrographs in polarized optical light of ''standard'' sample along flow direction.

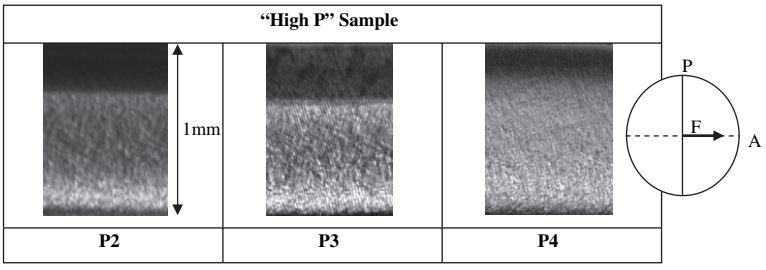

Fig. 7. Micrographs in polarized optical light of ''high P'' sample along flow direction.

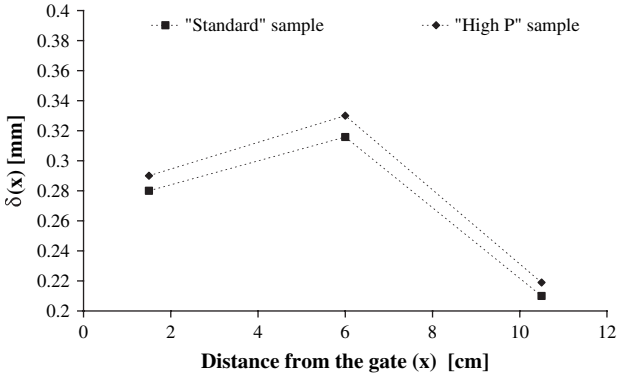

Fig. 8. Thickness of the oriented region $\delta(x)$, as a function of the distance from the gate, x.

constant along thickness in the whole sample for all molding tests.

2.5. Molecular orientation

2.5.1. Distribution along thickness direction

IR spectroscopy is also a very useful technique for the assessment of chain orientation, the procedure to determine the orientation is based on the dichroic ratio [3]. Results for the mixed amorphous-crystalline orientation, obtained by IR spectroscopy performed on samples cut according to scheme B, are reported in Fig. 13 for ''high P'' samples. In order to highlight the effects of operative conditions on orientation distribution along thickness, experimental data of molecular orientation

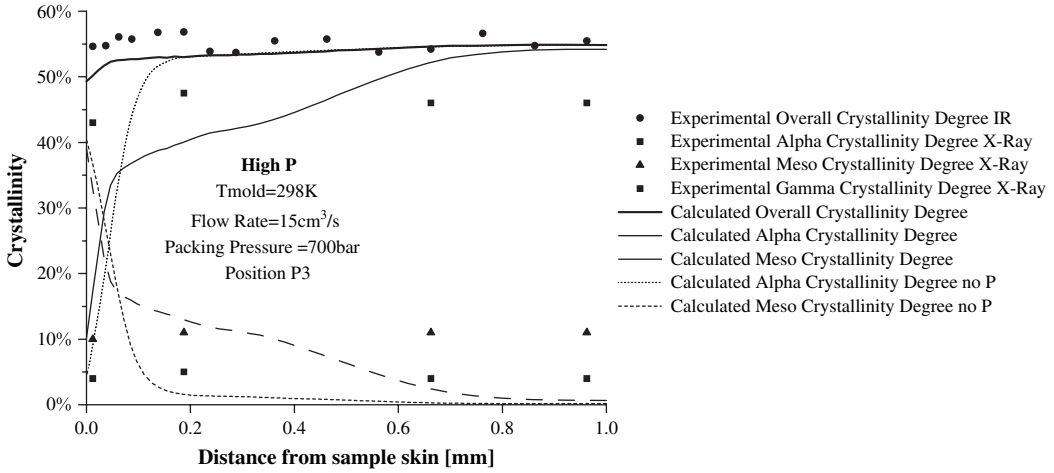

Fig. 9. Crystallinity distribution along thickness in P3 obtained by means of IR analysis and X-ray analysis (''high P'' sample).

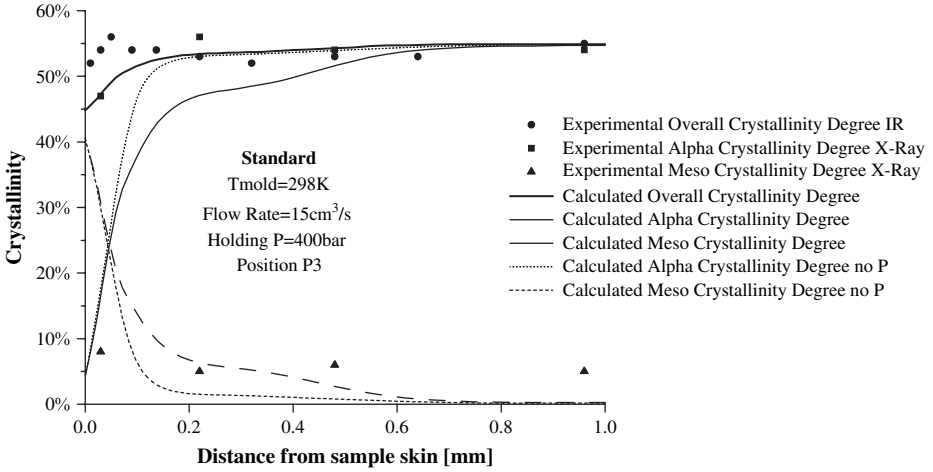

Fig. 10. Crystallinity distribution along thickness in P3 obtained by means of IR analysis and X-ray analysis (“standard” sample).

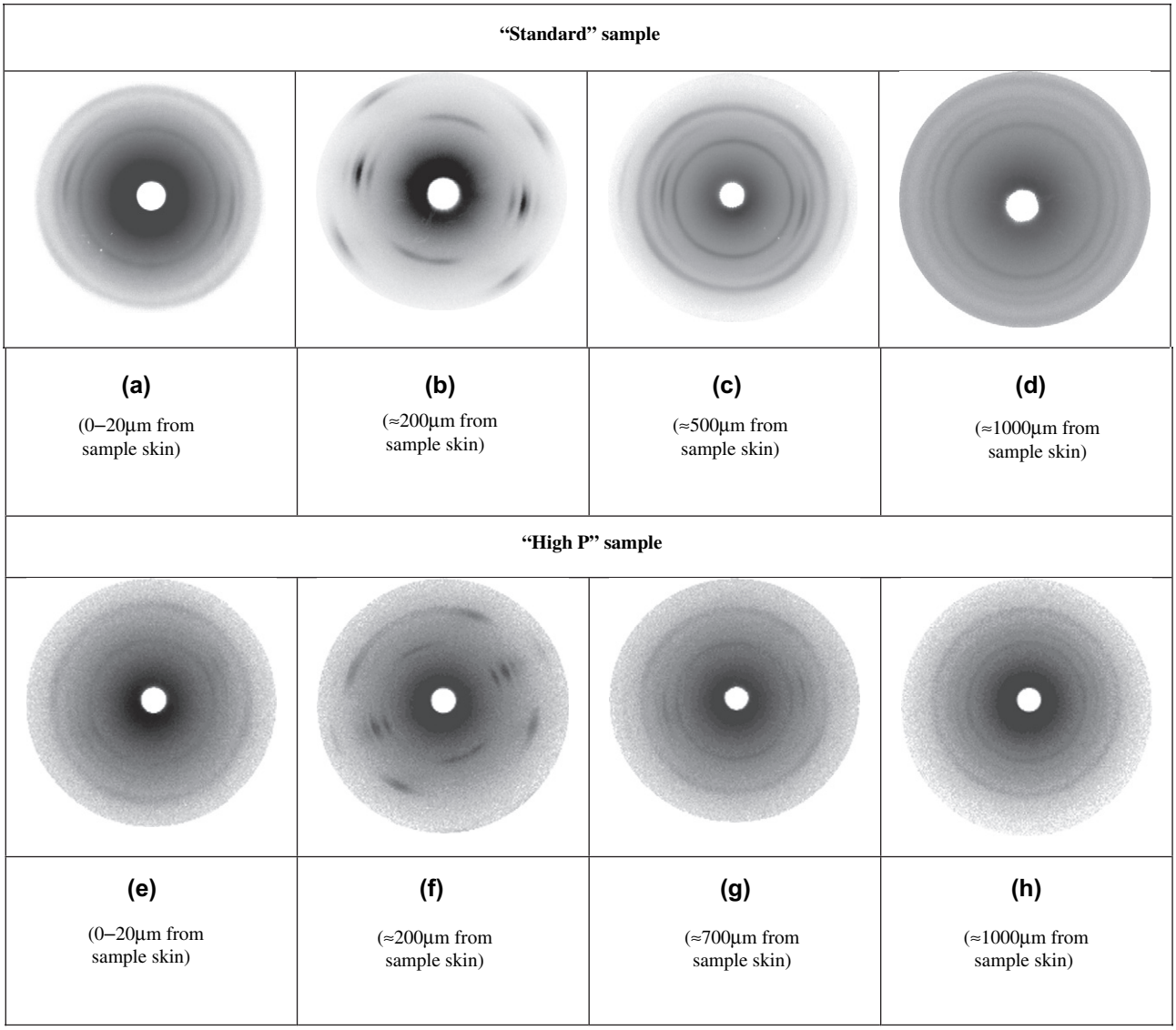

Fig. 11. Two-dimensional WAXD patterns for all samples analyzed.

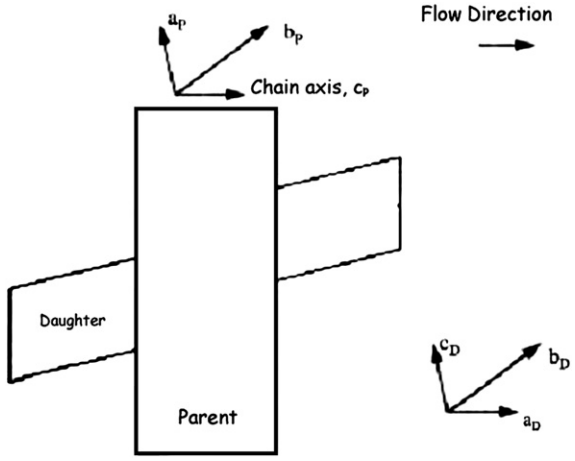

Fig. 12. A schematic model for the alignment of the parent and daughter lamellae in the oriented crystallites that explains the diffraction patterns in Fig. 11b and f.

in the ‘‘high P’’ samples are compared in the same figure with those in the ‘‘standard’’ sample.

Fig. 13 confirms a highly oriented zone in correspondence of the shear zone of Fig. 2a for both the samples analyzed. In the ‘‘standard’’ sample, after a maximum located in the shear zone, molecular orientation decreases monotonously on increasing the distance from the skin until the central zone is reached, where no preferred orientation is observed; in the ‘‘high P’’ sample, vice versa, orientation remains higher and even a second maximum at about 0.65 mm from the skin is observed. This maximum is normally associated to the effect of packing flow, which is much more effective in orienting the molecules [16].

Distribution along thickness of the angle between the direction of molecular orientation and the flow direction in P3 is reported in Fig. 14 for ‘‘standard’’ and for ‘‘high P’’ samples. The figure shows that for ‘‘standard’’ sample, orientation angle is smaller in layers close to the wall (about 5°), where orientation is higher, than in layers at the sample core (about

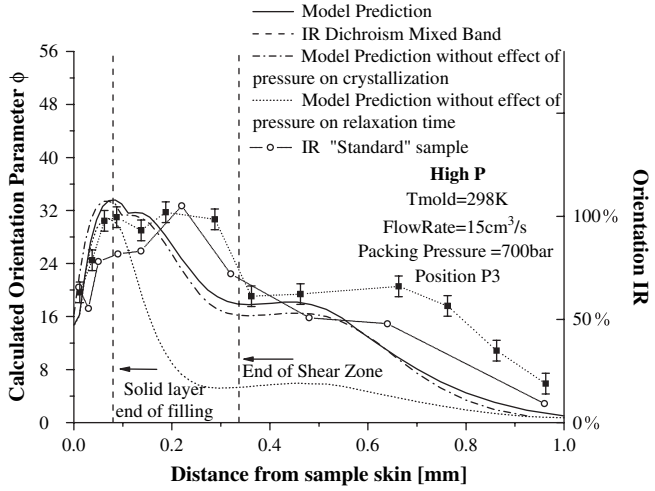

Fig. 13. Orientation distribution along thickness as determined by analysis of IR spectra for ‘‘high P’’ sample in P3. Results of simulations and results of ‘‘standard’’ sample are also shown.

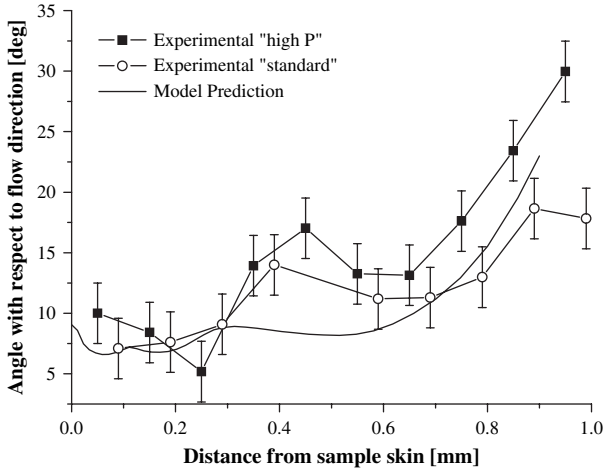

Fig. 14. Experimental and simulated distributions along thickness of the angle of average molecular orientation with respect to flow direction in ‘‘standard’’ and ‘‘high P’’ samples in P3.

25°). In the intermediate region (0.3–0.8 mm) the values are intermediate and essentially constant. In the ‘‘high P’’ sample the orientation angle undergoes a similar pattern with higher values in the region 0.7–1 mm from the skin. This difference is probably due to the packing flow, in fact, packing flow intensity and duration increase with holding pressure and, furthermore, the effect of flow on orientation is also enhanced by a pressure increase, as relaxation times increase with pressure.

In order to better clarify the relation between molecular orientation and orientation angle, the angle of average molecular orientation is reported as a function of the orientation in Fig. 15 for both experimental conditions analyzed in this work; also experimental results obtained from samples molded under different molding conditions including a higher mold temperature and a lower flow rate discussed elsewhere [3] are also reported in Fig. 15. As it can be seen, on decreasing orientation, the angle decreases.

2.5.2. Distribution along flow direction

In order to analyze molecular orientation along flow, IR analysis was performed on slices cut according to scheme B also in positions coded as P2 and P4 (1.5 and 10.5 cm from

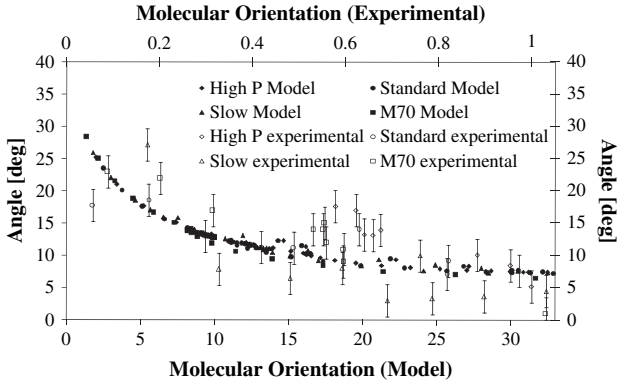

Fig. 15. Angle of average molecular orientation as function of orientation for both experimental data and model calculations.

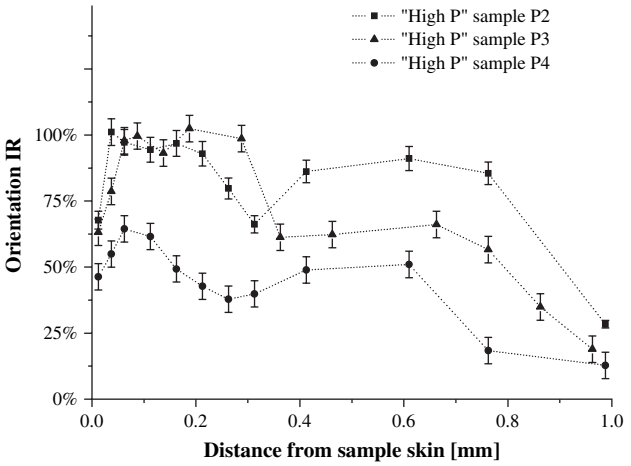

Fig. 16. Molecular orientation distribution along thickness in P2, P3 and P4 for "high P" sample.

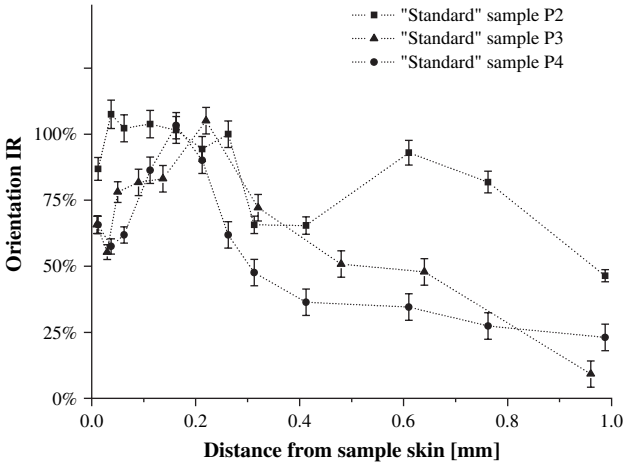

Fig. 17. Molecular orientation distribution along thickness in P2, P3 and P4 for "standard" sample.

the gate). Results obtained in P2 and P4 together with results obtained in P3 (6 cm from the gate) are reported in Figs. 16 and 17 for "high P" and "standard" samples, respectively.

Fig. 16 shows that orientation parameter in the "high P" sample, calculated by means of IR analysis, decreases on increasing the distance from the gate. Also in P2 and P4 the highest values are reached in correspondence with the shear band of Fig. 2. However, in the "high P" sample, orientation remains on high values in the whole thickness for all three positions considered showing a second maximum at about 0.6 mm from the skin. Also in "standard" sample the orientation parameter decreases on increasing the distance from the gate, but in this sample in P3 and P4 after the maximum an abrupt drop of molecular orientation takes place.

3. Modeling structure evolution

The process has been simulated using the software code developed at University of Salerno, which is based on Lord and Williams model and its extensions [17]. Further details about the model can be found elsewhere [3,18]. Material description in terms of PVT behavior and rheology can be found in Ref. [3]. Here it is worth noticing that both volume and viscosity depend on temperature, pressure and crystallinity degree (viscosity also depends on shear rate, obviously).

The goal of the simulation is the description of pressure evolution during the process and of the distributions of final crystallinity, molecular orientation and spherulite diameters.

3.1. Crystallization kinetics

In a recent paper, the effect of pressure in the quiescent crystallization kinetic model of the material here adopted for the experiments was described [8,9]. This model was adopted in the simulation code of the injection molding process; it considers a parallel two non-interacting kinetic processes competing for the available amorphous volume. The evolution of the volume fraction occupied by each of the crystalline phases, ξ_i, can thus be described by:

$$\frac{\mathrm{d}\xi_i}{\mathrm{d}t} = (1-\xi)\frac{\mathrm{d}k_i}{\mathrm{d}t} \tag{1}$$

where the subscript i stands for a particular phase (either for α or meso in this work).

$\xi_i = \chi_i/\chi_{\mathrm{m},i}$ where $\chi_{\mathrm{m},i}$ is the maximum volume fraction, which keeps into account the fact that growing crystals are always embedded into amorphous regions. $\xi = \sum_i \xi_i$ and k_i are the expected volume fractions of each phase if no impingement would occur.

The Kolmogoroff equation is adopted to describe the evolution of the volume fraction crystallized in the α form:

$$k_\alpha(t) = \frac{4\pi}{3}\int_0^t \frac{\mathrm{d}N(s)}{\mathrm{d}s}\left[\int_s^t G(u)\mathrm{d}u\right]^3 \mathrm{d}s \tag{2}$$

where N and G represent nucleation density and spherulitic growth rate, whose dependence upon temperature is described by the functions $N(s)$ (assuming heterogeneous nucleation) and $G(u)$ in Eq. (2) [19]:

$$N(T(t)) = N_0 \exp[\beta(T_\mathrm{m} - T(t))] \tag{3}$$

$$G[T(t)] = G_0 \exp\left[-\frac{U}{R(T(t)-T_\infty)}\right] \times \exp\left[-\frac{K_\mathrm{g}(T(t)+T_\mathrm{m})}{2T(t)^2(T_\mathrm{m}-T(t))}\right] \tag{4}$$

The evolution of the quiescent morphology, the density and dimensions of the spherulites, can be described on the basis of Eqs. (3) and (4). The effect of pressure on the nucleation density of the α-phase and the spherulitic growth rate were modeled by a shift of the melting and glass transition temperatures:

$$\begin{aligned} T_\mathrm{m} &= T_{\mathrm{m}0} + a(P-P_0) \\ T_\mathrm{g} &= T_{\mathrm{g}0} + b(P-P_0) \end{aligned} \tag{5}$$

where a and b are constant parameters and P_0 is the atmospheric pressure.

The final average dimensions of spherulites can be obtained from both the nucleation density and the degree of crystallinity. In fact, at least in quiescent conditions, the fractional crystallinity of the α-phase, ξ_α can be interpreted also as the volume fraction occupied by spherulites, per unit volume. The ratio between the fractional crystallinity and the number of active nuclei per unit volume is, therefore, an average measure of the final volume of spherulites. Correspondingly the final average radius of spherulites made of α crystallites can be calculated:

$$\overline{R} = \sqrt[3]{\frac{3\xi_{\alpha,\mathrm{final}}}{4\pi N_{\mathrm{a,final}}}} \quad N_{\mathrm{a,final}} = \int_0^{t_{\mathrm{final}}} \frac{\mathrm{d}N[T(s)]}{\mathrm{d}s}(1-\xi(s))\mathrm{d}s \tag{6}$$

where $N_{\mathrm{a,final}}$ is the final number of active nuclei [19].

The Avrami–Evans–Nakamura kinetic equation was adopted to describe the crystallization kinetics of the mesomorphic form. Thus, the evolution of the undisturbed volume of the mesomorphic phase is described as:

$$k_{\mathrm{meso}}(t) = \ln 2 \left[\int_0^t B(T(s))\mathrm{d}s\right]^n \tag{7}$$

where n is the Avrami index and $B(T)$ a kinetic constant, which, on the basis of so-called isokinetic assumption, is simply described by a Gaussian shaped curve (D, $T_{\max}$ and $K_{\max}$ are the half width of the Gaussian curve, the temperature at which the maximum of $B(T)$ is attained, and the maximum value itself, respectively):

$$B(T) = K_{\max} \exp\left[-4\ln 2 \frac{(T-T_{\max})^2}{D^2}\right] \tag{8}$$

Also in the crystallization kinetics of the mesomorphic phase the effect of pressure was accounted for assuming that $T_{\max}$ and $K_{\max}$ depend on pressure according to the following relationships:

$$\begin{aligned} T_{\max} &= T_{\max 0} + c(P-P_0) \\ K_{\max} &= K_{\max 0} \exp[d(P-P_0)] \end{aligned} \tag{9}$$

The values of parameters previously identified on the basis of independent tests on samples crystallized under quiescent conditions in a wide range of cooling rates and pressures [8,9] are reported in Table 2.

As already reported, in our experiments, the percentage of the γ-phase does not exceed 5%; this phase was thus not considered in the crystallization kinetics model.

3.2. Molecular orientation

The software code adopted allows to calculate the evolution of molecular orientation by applying a simple dumbbell model on the basis of kinematics obtained by a viscous approach [20]. According to this model, the constitutive equation for the subchain population described by the tensor $\underline{\underline{A}}$ can be written as:

$$\frac{D}{Dt}\underline{\underline{A}} - \underline{\underline{\nabla v}}^T\,\underline{\underline{A}} - \underline{\underline{A}}\,\underline{\underline{\nabla v}} = -\frac{1}{\lambda}\underline{\underline{A}} + \underline{\underline{\nabla v}} + \underline{\underline{\nabla v}}^T \tag{10}$$

where $\nabla \underline{v}$ is the velocity gradient and λ is the relaxation time. Once the velocity field is known, Eq. (10) presents a single parameter, the relaxation time, λ, which, in this work, was allowed to be function of shear rate ($\dot\gamma$), temperature, pressure and crystallinity, according to the equations:

$$\lambda(T,P,\gamma',\chi) = \frac{\lambda^*\alpha'(T,P,\chi)}{1+E[\lambda^*\alpha'(T,P,\chi)\gamma']^{1-b}} \tag{11}$$

$$\alpha'(T,P,\chi) = 10^{-\frac{F_1(T-B_1-B_2P)}{F_2+T-B_1}} h'_\chi(\chi) \tag{12}$$

$$h'_\chi(\chi) = \left[1 + e_1 \exp\left(-\frac{e_2}{\chi^p}\right)\right] \tag{13}$$

The values of the parameters adopted to describe the relaxation time were obtained in a previous work on the basis of viscoelastic measurements [3] and they are reported in Table 3.

It is worth mentioning that, according to the model depicted above, material viscoelastic behavior is described with the use

Table 3
Values of the parameters adopted to describe the viscoelastic behavior of iPP T30G (Eqs. (11)–(13))

Parameter	Value	Parameter	Value
F_1	2.5	e_1	6.12×10^{13}
F_2	301.4 K	e_2	12.32
E	3.5	p	0.18
b	0.23		
λ^*	14 s		
B_1	503 K		
B_2	0.17 K/bar		

Table 2
List of parameters adopted in the kinetic model

Parameter	Value	Parameter	Value	Parameter	Value
N_0	17.4×10^6 nuclei/m^3	D	38.3 K	a	0.016 K/bar
β	0.155 K^{-1}	$\chi_{\mathrm{m,meso}}$	0.44	b	0.031 K/bar
K_g	534,858 K^2	$T_{\max}$	318 K	c	0.045 K/bar
$\chi_{\mathrm{m},\alpha}$	0.55	$K_{\max 0}$	4.4 s^{-1}	d	−0.002 l/bar
G_0	2.1×10^{10} μm/s	n	2.83		
$T_{\inf}$	236 K				
U/R	755 K				

of only one relaxation time. However, since relaxation time is taken as a function of shear rate, it essentially describes a series of infinite relaxation modes, each one playing a role at a given shear rate.

4. Discussion on results and simulation results

4.1. Pressure curves

Simulated and experimental pressure curves for all transducers are reported in Fig. 1. Results show that pressure evolution was satisfactorily described at all transducer positions. Also the gate freeze-off time was nicely described by the model for both standard and high pressure conditions. This was taken as an evidence that the code well describes all relevant features of thermomechanical history experienced by the polymer during the molding tests.

The description of pressure curves for the standard test does not change significantly on neglecting the effect of pressure on crystallization. Results of the simulation software in the original formulation (neglecting the effects of pressure on crystallization) are not given in the figures. However, as far as "high P" samples is concerned, once the effect of pressure on crystallization is neglected, the model description of the pressure evolution worsens, especially during the cooling step, when the slopes predicted by the model became significantly steeper than experimental results.

4.2. Average spherulite diameter distribution along thickness

Model predictions for spherulite diameters in P3 are compared with experimental data in Fig. 5 for the "high P" samples. Description of data is satisfactory in internal layers (closer to the midplane); of course the (quiescent) crystallization model predicts the presence of spherulites also in the shear zone (whose thickness is marked by a vertical dotted line in the figures) where SEM and AFM analyses revealed that spherulitic structures are replaced by fiber like structures. In agreement with experimental observations, the biggest spherulites are predicted in the core region and become smaller going from the core region toward the skin. This can be associated with the evolution of temperature profile during the process: spherulites at the locations closer to the mold wall undergo very high cooling rates, spherulite growth does not have time to proceed, nucleation density becomes large and final spherulite dimensions remain small, because limited by impingement. At the locations close to the centre, cooling rate is much smaller, spherulites have time to grow with low nucleation density and reach larger dimensions before impingement.

4.3. Crystallinity distribution along thickness direction

A comparison between experimental data and model predictions of the relative amount of the phase distribution along thickness direction of the moldings is considered in Fig. 9 for "high P" sample and in Fig. 10 for "standard" samples, respectively. Model predictions of distribution of crystalline phases obtained by neglecting the effect of pressure on crystallization kinetics are also shown in the figures.

The final overall crystallinity distribution nicely compares with experimental results as it is essentially constant along the thickness.

Figures show that the kinetic model describes the increase of the ratio between the mesomorphic phase and the α-phase with the high pressures. This effect is particularly evident near the skin (high cooling rate) and less evident in the central layers (low cooling rates), whilst experimental data seem to indicate that the effect of pressure is relevant also in the central layers (low cooling rates). It comes out from this comparison that in the shear layer, orientation induces an enhancement of crystallization kinetics of the α-phase, which develops also in the skin layers.

4.4. Molecular orientation

4.4.1. Distribution along thickness direction

The maximum eigenvalue of the deformation tensor A, denoted by ϕ in the present work, is a suitable index of molecular orientation. Comparison between experimental and predicted distribution of molecular orientation along thickness direction in pos. P3 is reported in Fig. 13. Results well predict a highly oriented zone in correspondence with the shear zone for all samples analyzed and a pronounced maximum close to the position of the last layers which solidify during filling. In the same figure a dotted vertical line indicates the position of the last layer which solidifies during the filling step; solidification condition being identified when the overall crystallinity degree reaches 1%. It is worth noticing that the shear zone is thicker than the layers solidified during filling.

Similar to the behavior shown by the experimental IR dichroic ratio, model predictions present an intermediate plateau at distances from the skin larger than 0.3 mm. This plateau is determined by the increase of relaxation time taking place during the packing flow by effect of both temperature decrease and pressure increase.

The importance of the effect of pressure on relaxation time is clearly shown in Fig. 13, where also orientation predictions obtained neglecting the effect of pressure on relaxation time are reported. Neglecting the effect of pressure on relaxation time gives rise to an enormous effect on model predictions and the experimental features are not reproduced anymore. Indeed, in such case, predictions decrease to small values already at very small distances from the skin.

Fig. 13 shows also that, in order to describe molecular orientation distribution, the effect of pressure on crystallization kinetics is secondary with respect to the effect of pressure on relaxation time, particularly in layers solidified during the packing.

4.4.2. Distribution along flow direction

Comparison between experimental and predicted distributions of molecular orientation along thickness direction in

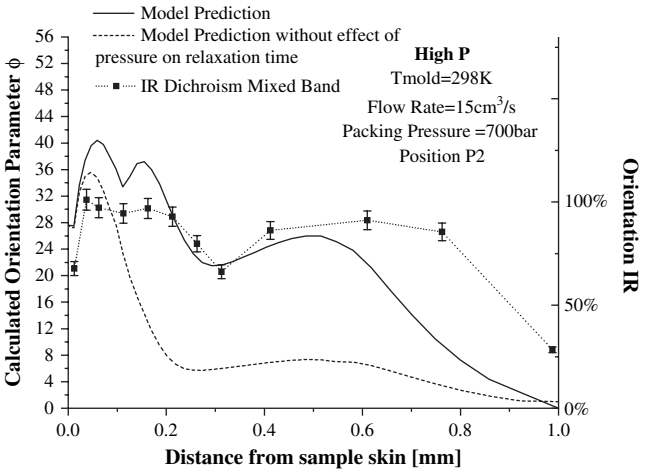

Fig. 18. Orientation distribution along thickness as determined by analysis of IR spectra for ''high P'' sample in P2. Results of simulations are also shown as full lines.

the other positions (P2 and P4) for the ''high P'' sample is reported in Fig. 18 (P2) and Fig. 19 (P4). Results well predict that orientation parameter decreases on increasing the distance from the gate. At long distances the time the material undergoes filling flow becomes shorter and the packing flow rate reduces; both conditions contribute to keep molecular orientation low. The model well predicts the highly oriented zone in correspondence with the shear zone for all samples analyzed and is also able to describe the maximum present at intermediate distances from the skin in position P2 for all samples.

4.5. Direction of orientation

A comparison between experimental and predicted distributions along thickness of the angle in position P3 between direction of molecular orientation and main flow direction is reported in Fig. 14. Model predictions are less sensitive to molding conditions with respect to experimental data. However, the main features of experimental results are captured. Also simulation results indicate that the orientation direction is closer to the main flow direction on increasing levels of orientation.

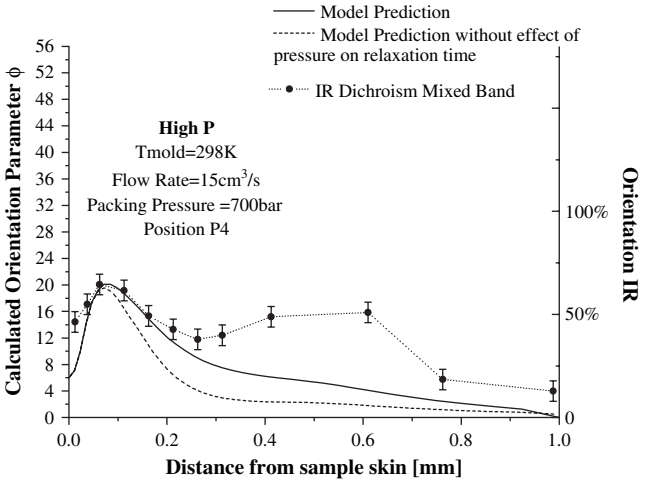

Fig. 19. Orientation distribution along thickness as determined by analysis of IR spectra for ''high P'' sample in P4. Results of simulations are also shown as full lines.

5. Conclusions

Injection molding tests were performed under different conditions; in particular, in order to study effects of packing pressure on morphology distribution, different holding pressures were adopted. The resulting morphology of the moldings was characterized by adopting different experimental techniques and, in order to underline the effects of holding pressure, it was compared with previous results. Data of molecular orientation underline the effect of packing flow, in fact, in the ''standard'' sample, molecular orientation decreases on increasing the distance from the skin until the central zone is reached, where a preferred orientation is not present, whilst in the ''high P'' sample, orientation remains on high values in the whole thickness; even a second maximum is observed. Furthermore, even if the overall crystalline content inside the sample remains the same for all the conditions analyzed, a sensible reduction of the percentage of α-phase is found on increasing the holding pressure, whereas the percentage of mesomorphic phase increases and a small fraction of γ-phase is found, which was not present in the samples molded at lower holding pressures.

Morphological characteristics of the samples were also compared with the predictions of a simulation code developed at University of Salerno. For this purpose, the quiescent crystallization kinetics model was modified in order to take into account the effect of pressure on crystallization according to literature. The simulation code satisfactorily describes experimental data of pressure evolution and crystallinity and orientation distribution along the thickness of the sample. By comparing the simulation results with the experimental observations, interesting conclusions regarding the effect of pressure could be drawn. For instance, it was shown that, concerning the evolution of pressure and molecular orientation, the effect of pressure on crystallization kinetics is certainly negligible with respect to the effect of pressure on viscosity (which is also strongly depending on crystallinity). On the other hand, the distribution of the different crystalline phases is highly influenced by the effect of the pressure on the kinetics.

References

[1] Cakmak M, Hsiung CM, Wang YD. Structure development in injection molding of semicrystalline polymers. Shiguma Syuppan Publisher; 1997.
[2] Shonaike GO, Advani SG. Advanced polymeric materials: structure–property relationship. CRC Press; 2003.
[3] Pantani R, Coccorullo I, Speranza V, Titomanlio G. Prog Polym Sci 2005;30:1185–222.
[4] Guo X, Isayev AI, Demiray M. Polym Eng Sci 1999;39:2132–49.
[5] Zhu P, Edward E. Polymer 2004;44:2603–13.
[6] Angelloz C, Fulchiron R, Douilard A, Chabert B, Fillit R, Vautrin A, et al. Macromolecules 2000;33:4138–45.

[7] Meille SV, Phillips PJ, Mezghani K, Bruckner S. Macromolecules 1996; 29:795–9.
[8] Coccorullo I, Pantani R, Titomanlio G. Polymer 2003;44:307–18.
[9] Coccorullo I, Pantani R, Titomanlio G. Int Polym Process 2005;XX: 186–90.
[10] Pantani R, Speranza V, Titomanlio G. Polym Eng Sci 2001;41:61–71.
[11] Pantani R, De Santis F, Brucato V, Titomanlio G. Polym Eng Sci 2004; 44:1–17.
[12] White HM, Basset DC. Polymer 1998;39:3211–20.
[13] Samuels RJ. Structured polymer properties. New York: John Wiley & Sons; 1974.
[14] La Carrubba V, Brucato V, Piccarolo S. Polym Eng Sci 2000;40: 2430–41.
[15] Murthy NS, Minor H. Polymer 1990;31:996–1002.
[16] Pantani R, Sorrentino A, Speranza V, Titomanlio G. Rheol Acta 2004;43: 109–18.
[17] Lord HA, Williams G. Polym Eng Sci 1978;18:314–20.
[18] Titomanlio G, Speranza V, Brucato V. Int Polym Proc 1997;12:45–53.
[19] Eder G, Janeschitz-Kriegl H. Materials science and technology 18. Wiley Company; 1997.
[20] Pantani R, Speranza V, Sorrentino A, Titomanlio G. Macromol Symp 2002;185:293–307.